AIAA AVIATION Forum
June 15-19, 2020, VIRTUAL EVENT
AIAA AVIATION 2020 FORUM

10.2514/6.2020-3131

Towards Adjoint-based Sensitivity Analysis for Supersonic Jet Noise

Enrico Fabiano * Zhi Yang † Dimitri Mavriplis ‡

Scientific Simulations, LLC, Laramie, WY 82072-5007.

Asitav Mishra §

National Institute of Aerospace, Hampton, VA 23666.

This paper presents a formulation for the sensitivity analysis of supersonic jet noise. Using an acoustic-analogy approach, an unstructured, steady-state, Reynolds-Averaged Navier-Stokes (RANS) solution is used to assemble the jet's acoustic sources and compute the far-field spectra for observers at right angles to the jet. Both forward and adjoint formulations are derived that correspond to analogues of the aeroacoustic analysis problem. Adjoint-based shape optimization is used to minimize the farfield acoustic signature of the jet, without compromising the aeropropulsive performance of the nozzle.

I. Introduction

Commercial supersonic flight has experienced renewed interest in recent years and promises to significantly reduce travel time, particularly for international trips. Before entering service, however, the next generation of supersonic commercial aircraft will have to comply with ever more stringent noise regulations. While many research efforts have focused on understanding sonic boom generation,[1] its prediction,[2–4] and its mitigation,[5,6] the noise generated by aircraft configuration at take-off and landing has received less attention. During these flight phases the acoustic signature of the aircraft is dominated by airframe, fan and jet noise. Jet noise is of particular interest because of its dominant contribution to the noise radiated from the aircraft at take-off. The design of a supersonic engine nozzle is a challenging multidisciplinary problem since compliance with noise regulations at low subsonic speeds must not compromise the thrust required to sustain commercial supersonic flight.

The nozzle shape design problem has traditionally been treated with low-fidelity empirical models, often focusing on either the aeroacoustic or the aerodynamic performance individually. Although eddy-resolving CFD methods for computing high-speed jet noise are now available,[7,8] such methods are computationally expensive and are considered impractical for use in a design optimization environment. On the other hand, the prediction of turbulence generated noise using the steady-state RANS equations provides a less accurate but more cost-effective approach for practical design problems. Using an acoustic-analogy formulation, the jet noise sources are extracted from a near-field steady RANS solution and propagated to the far-field observer. Recently, these hybrid CFD-CAA approaches have been used for the computation of the aerodynamic and acoustic performance metric of the nozzle,[9] and have been shown to successfully predict the variation of the aeroacoustic performance metric in response to a geometric variation of the nozzle shape.[10] However, while cheaper than eddy-resolving methods, these acoustic-analogy approaches are significantly more expensive than traditional empirical models, and their application to large-scale multidisciplinary design problems requires the use of efficient numerical optimization techniques. Gradient-based methods can be used to solve these large-scale design problems provided that the sensitivity of the objective to the design variables can be efficiently computed. The use of adjoint-based approaches allows for the computation of the objective function's sensitivities at a cost independent of the number of design variables, enabling the use of gradient-based methods for multidisciplinary design problems. Originally developed for aerodynamic design problems,[11] adjoint-based methods have been extended to treat aerostructural,[12–14] aeroacoustic[5,15–17] and aero-structural-acoustic[18] problems. However,

*Research engineer; enrico@scientific-sims.com
†Senior Research Scientist; PI; zyang@scientific-sims.com
‡Professor (UWYO); Senior Technical Specialist; mavripl@scientific-sims.com
§Research Engineer II; asitav.mishra@nianet.org

application of adjoint methods to jet noise problems has been scarce. This paper presents the development and application of an adjoint-based sensitivity analysis for jet noise minimization based on a simplified acoustic-analogy approach. An unstructured steady RANS solution around the nozzle is used to assemble the jet acoustic sources and compute the far-field noise spectra of the jet, following a similar approach to that described in the work by Bridges.[19] The forward and adjoint linearizations of the aeroacoustic problem are derived by hand differentiation of the coupled CFD-CAA approach, and the adjoint linearization is used by a gradient-based optimization algorithm to minimize the noise of the jet without compromising the nozzle aeropropulsive performance. The paper is structured as follows: section II introduces the steady RANS flow solver used in this work and its discrete adjoint sensitivity formulation, while section III discusses the simplified acoustic-analogy approach used for jet noise prediction. Section IV presents the geometry parameterization used for optimization of the nozzle shape. Section V presents jet noise optimization results. Furthermore, the noise reductions identified with the acoustic-analogy approach proposed in this work are evaluated using NASA's JeNo code[9,20,21] as part of an ongoing development effort to develop an adjoint-based jet noise design optimization capability using JeNo. Finally, section VI draws conclusion and highlights future work.

II. Aerodynamic Analysis and Sensitivity Formulation

A. Flow Solver Analysis Formulation

The base flow solver used in this work is the NSU3D unstructured mesh Reynolds-averaged Navier-Stokes solver. NSU3D has been extensively applied to steady-state and time-dependent flows and contains a discrete tangent and adjoint sensitivity capability. Hence, only a concise description of these formulations will be given in this paper, with additional details available in previous references.[13,22–24] The flow solver is based on the conservative form of the Navier-Stokes equations which may be written as:

$$\frac{\partial \mathbf{U}(\mathbf{x},t)}{\partial t} + \nabla \cdot \mathbf{F}(\mathbf{U}) = 0 \tag{1}$$

where the state vector $\mathbf{U}$ consists of the conserved variables and the Cartesian flux vector $\mathbf{F} = (\mathbf{F}_x, \mathbf{F}_y, \mathbf{F}_z)$ contains both inviscid and viscous fluxes. The equations are closed with the perfect gas equation of state and the $k-\omega$ turbulence model for all cases presented in this work. The solver uses a vertex-centered median dual control volume formulation that is second-order accurate, where the flux integral around a closed control volume is discretized as:

$$\mathbf{R}(\mathbf{U}) = \int_{\mathbf{dB(t)}} [\mathbf{F}(\mathbf{U})] \cdot \mathbf{ndB} = \sum_{\mathbf{i=1}}^{\mathbf{n_{edge}}} \mathbf{F}^{\perp}_{\mathbf{e_i}}(\mathbf{U}, \mathbf{n_{e_i}}) \mathbf{B_{e_i}} = \mathbf{0} \tag{2}$$

where B_e is the face area, $\mathbf{n}_e$ is the unit normal of the face, and $F_e^{\perp}$ is the normal flux across the face. The normal flux across the edge is computed using the second-order accurate matrix dissipation scheme[25] as the sum of a central difference and an artificial dissipation For the case of steady-state flows considered in this work, the time derivative term in equation (1) represents a pseudo-time term used to facilitate convergence to the steady-state solution. After the residual vector $\mathbf{R}$ is linearized with respect to the unknown flow solution vector $\mathbf{U}$, the system of nonlinear equations (2) is solved for using Newton's method as:

$$\begin{aligned} \left[\frac{\partial \mathbf{R}^k}{\partial \mathbf{U}^k}\right] \delta \mathbf{U}^k &= -\mathbf{R}^k \\ \mathbf{U}^{k+1} &= \mathbf{U}^k + \delta \mathbf{U}^k \\ \delta \mathbf{U}^k \rightarrow 0, \mathbf{U}^n &= \mathbf{U}^k \end{aligned} \tag{3}$$

The Jacobian matrix is inverted iteratively using a line-implicit agglomeration multigrid scheme that is applied as a preconditioner for a GMRES Krylov solver.[26]

The flow around the SMC006 nozzle[27] is used to validate the NSU3D flow solver for jet-flow applications. The nozzle is axisymmetric and is augmented with 6 triangular chevrons. The flow conditions correspond to Set Point 7 from the Tanna Matrix.[28] The nozzle pressure ratio is $p_0/p_\infty = 1.861$, the temperature ratio $T_0/T_\infty = 1$ and the jet Mach number is $M_j = 0.985$. A freestream Mach number $M_\infty = 0.01$ is imposed as a freestream boundary condition to facilitate the convergence of the flow solver[29] and the Reynolds number based on the freestream Mach number and the $2in$ nozzle diameter is $Re = 5789.0/in$. The unstructured CFD mesh used to simulate the flow around the nozzle is shown in Fig. 1(a). The mesh consists of approximately 2.34 million nodes and is refined near the nozzle exit to better

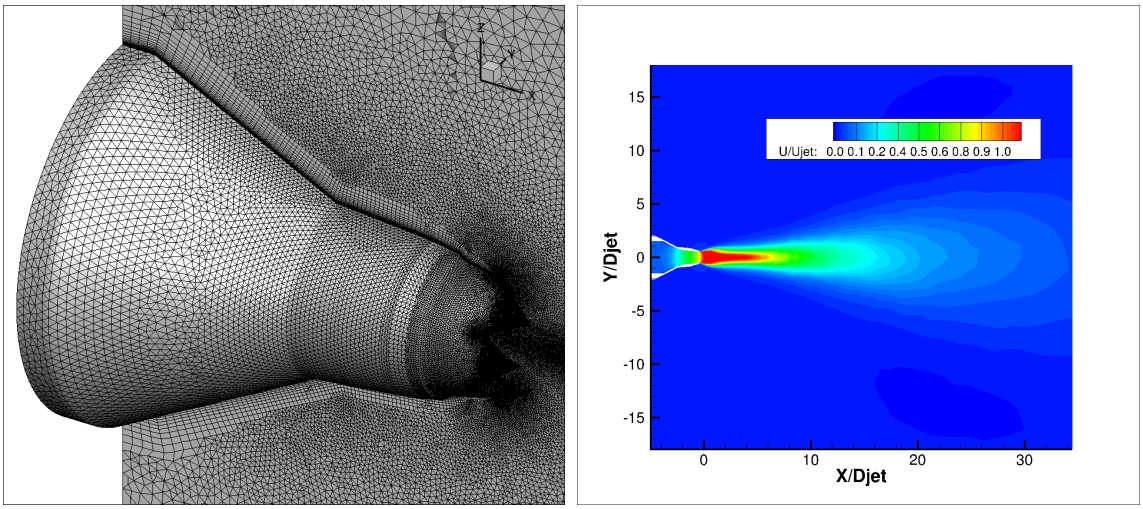

(a) Unstructured CFD mesh (b) Computed streamwise velocity contours

Figure 1. Unstructured CFD mesh around the SMC006 nozzle geometry and streamwise velocity contours for the $\kappa-\omega$ RANS solution

resolve the jet shear layer. Figure 1(b) shows the nozzle jet plume computed with the $\kappa-\omega$ turbulence model, while a comparison between computed and experimental[27] contours of total pressure coefficient at several streamwise stations is shown in Fig. 2. The good agreement between the computed and experimental flowfields validates our aerodynamic

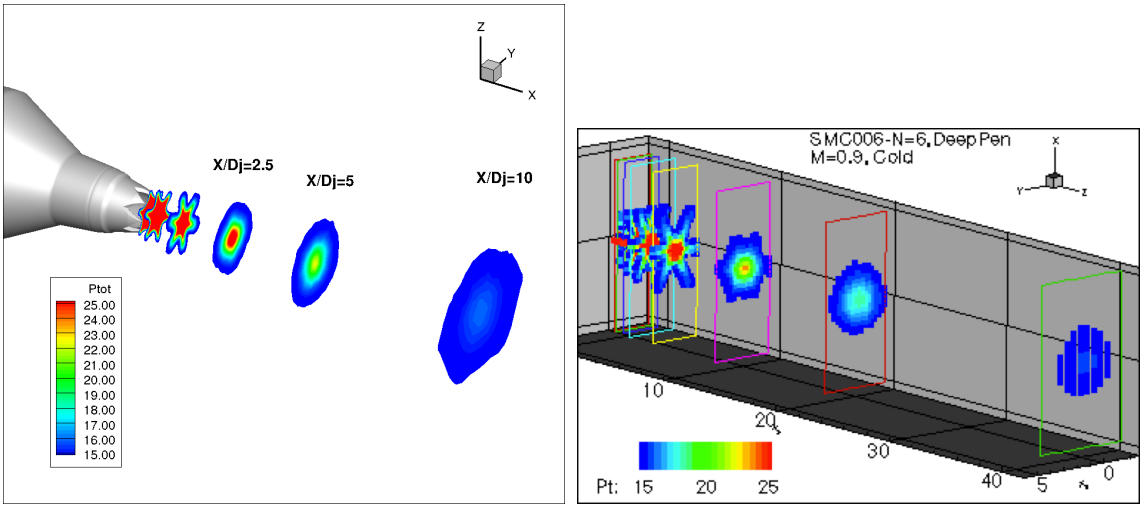

(a) Contours of computed total pressure coefficient at different streamwise stations (b) Contours of experimental total pressure coefficient at different streamwise stations[27]

Figure 2. Validation of the NSU3D $\kappa-\omega$ computations for the SMC006 nozzle geometry

analysis and is essential for the accurate prediction of the noise generated by the nozzle.

B. Mesh deformation capability

In order to apply the optimal shape changes computed by the optimization algorithm, a mesh deformation strategy must be employed. In this approach, the mesh is modeled as a linear elastic solid with a variable modulus of elasticity that can be prescribed either as inversely proportional to cell volume or to the distance of each cell from the nearest wall.[30,31] The resulting equations are discretized and solved on the mesh in its original undeformed configuration in response to surface displacements using a line-implicit multigrid algorithm analogous to that used for the flow

equations. The governing equations for mesh deformation can be written symbolically as:

$$\mathbf{G}(\mathbf{x}, \mathbf{x_{surf}}(\mathbf{D})) = \mathbf{0} \tag{4}$$

where $\mathbf{x}$ denotes the interior mesh coordinates and $\mathbf{x_{surf}}(\mathbf{D})$ are the surface mesh coordinates that depend on the shape parameters that define the surface geometry.

C. Aerodynamic Sensitivity Analysis Formulation

The sensitivity analysis implementation follows the strategy developed in references.[22,23] The objective function L is evaluated using the steady flow and mesh solution, $\mathbf{U}$ and $\mathbf{x}$ respectively, as:

$$L = L(\mathbf{U}, \mathbf{x}) \tag{5}$$

Assuming that the state variables, i.e., $\mathbf{U}, \mathbf{x}$, are dependent on some input design parameters $\mathbf{D}$, the total sensitivity of the objective function L to a design variable D can be expressed as the inner product between the vector of state sensitivities to the design input and the vector of objective sensitivities to the state variables as:

$$\frac{dL}{dD} = \begin{bmatrix} \frac{\partial L}{\partial \mathbf{x}} & \frac{\partial L}{\partial \mathbf{U}} \end{bmatrix} \begin{bmatrix} \frac{d\mathbf{x}}{dD} \\ \frac{d\mathbf{U}}{dD} \end{bmatrix} \tag{6}$$

The non-linear flow residual operator and the linear elasticity mesh residual operator described earlier provide the constraints for the sensitivity analysis:

$$\begin{aligned} \mathbf{G}(\mathbf{x}, \mathbf{D}) &= 0 \\ \mathbf{R}(\mathbf{U}, \mathbf{x}) &= 0 \end{aligned} \tag{7}$$

and their linearization with respect to the design variable yields:

$$\begin{bmatrix} \frac{\partial \mathbf{G}}{\partial \mathbf{x}} & 0 \\ \frac{\partial \mathbf{R}}{\partial \mathbf{x}} & \frac{\partial \mathbf{R}}{\partial \mathbf{U}} \end{bmatrix} \begin{bmatrix} \frac{d\mathbf{x}}{dD} \\ \frac{d\mathbf{U}}{dD} \end{bmatrix} = \begin{bmatrix} -\frac{\partial \mathbf{G}}{\partial D} \\ 0 \end{bmatrix} \tag{8}$$

Upon solution of the forward sensitivity equation (8), the mesh and flow sensitivity vectors can be substituted into equation (6) to obtain the complete sensitivity of the objective L with respect to the design variable D. Hence, the forward sensitivity approach requires a new solution of equation (8) for each design parameter D. On the other hand, the adjoint approach can obtain the sensitivities for any number of design inputs $\mathbf{D}$ at a cost approximately independent of the number of design variables. The adjoint formulation can be obtained by transposing the tangent linearization in equation (8), resulting in equation (9)

$$\begin{bmatrix} \frac{\partial \mathbf{G}}{\partial \mathbf{x}}^T & \frac{\partial \mathbf{R}}{\partial \mathbf{x}}^T \\ 0 & \frac{\partial \mathbf{R}}{\partial \mathbf{U}}^T \end{bmatrix} \begin{bmatrix} \Lambda_{\mathbf{x}} \\ \Lambda_{\mathbf{U}} \end{bmatrix} = \begin{bmatrix} \frac{\partial L}{\partial \mathbf{x}}^T \\ \frac{\partial L}{\partial \mathbf{U}}^T \end{bmatrix} \tag{9}$$

where $\Lambda_{\mathbf{U}}$ and $\Lambda_{\mathbf{x}}$ are the flow and mesh adjoint variables respectively. The final objective sensitivities can then be obtained as:

$$\frac{dL}{d\mathbf{D}}^T = \begin{bmatrix} \frac{\partial \mathbf{G}}{\partial \mathbf{D}}^T & 0 \end{bmatrix} \begin{bmatrix} \Lambda_{\mathbf{x}} \\ \Lambda_{\mathbf{u}} \end{bmatrix} \tag{10}$$

A more detailed description of the complete formulation is presented in reference.[22]

III. Aeroacoustic model: Analysis and Sensitivity Formulation

Despite the continuous increase in computational resources, jet noise design optimization strategies based on scale-resolving acoustic-analogy approaches are still infeasible. A viable approach to nozzle design optimization is the use of RANS-based hybrid methods that have been developed over the years and are now fairly well established.[10,19,32–34] These hybrid methods use a finely resolved near-field steady RANS solution to predict the noise radiated from the jet to a given observer using an acoustic-analogy formulation.

The acoustic formulation proposed in this work uses a steady RANS solution to assemble the noise sources and computes an approximate far-field noise spectra for observers at right angles to the jet. The RANS solution is computed using a two-equation turbulence model in the NSU3D flow solver and the acoustic sources are derived following the approach described in.[20,21,33] For gradient-based shape optimization, the linearization of the proposed acoustic formulation is coupled to the linearization of the flow solver to compute of sensitivity of the acoustic objective function with respect to the full vector of design variables.

The acoustic analogy proposed in this work lays the foundation for the implementation of an efficient nozzle design optimization strategy based on the JeNo[33,35] jet noise prediction software.

A. Acoustic analysis formulation

In the proposed acoustic-analogy approach, the turbulent flow field around the nozzle is computed by the unstructured NSU3D RANS solver using the $\kappa-\omega$ turbulence closure. The steady RANS solution around the nozzle is used to compute the axial component of the two-point fourth-order velocity correlations[20,21,33] at each CFD volume mesh node as:

$$I_{1111}(\omega^s) = A_m \kappa^{7/2} \frac{\tau_0^4}{1+(\omega^s \tau_o/2)^2} N(k\ell) \tag{11}$$

where κ is the acoustic source turbulent kinetic energy as computed by the turbulence model, τ_0 is the source turbulent timescale, $N(k\ell)$ is the source non-compactness factor and ω^s is the source frequency. The acoustic source time and length scale are derived by the $\kappa-\omega$ RANS solution as:

$$\begin{aligned} \tau_o &= c_\tau / \left(\beta^+ \omega\right) \\ \ell &= c_\ell \kappa^{1/2} / \omega \end{aligned} \tag{12}$$

The terms A_m, c_τ and c_ℓ are calibration constants in the two-point, fourth-order velocity coorrelation, while $\beta^+ = 0.09$ is a calibration constant in the $\kappa-\omega$ turbulence model. The source non-compactness factor [20,33] is computed as:

$$N(k\ell) = exp(-\frac{k^2\ell^2}{8\pi}) \tag{13}$$

Here k is the acoustic wave number defined as $k = \Omega/c_\infty$, where Ω is the observer frequency and c_∞ is the freestream speed of sound. The source and observer frequencies are related through the Doppler factor $\omega^s = \Omega(1 - M_c cos\theta)$, where M_c is the convective Mach number. In the present work the acoustic observer is located at a polar angle of $\theta = 90$ deg from the streamwise jet axis, so that $\Omega = \omega^s$. The noise source term in equation (11) is then integrated over the jet volume that radiates directly to the far field for every observer frequency of interest:

$$PSD(\omega^s) = \int_{Jet\ Vol} I_{1111}(\omega^s) dVol \tag{14}$$

The integration volume in equation (14) is cylindrical in shape and extends from the nozzle exit to 20 jet diameters downstream, with a radius of 1.5 jet diameters. Every CFD node in this region is an acoustic source, and the nodal turbulent solution is used to assemble equation (11) for the desired observer frequency. The approximate acoustic spectra at the observer, equation (14), is integrated over multiple frequencies in the range of jet Strouhal number $St = 0.1 - 10$ to form the acoustic objective that will be targeted during the nozzle design optimization as:

$$L_{acou} = \sum_{\omega^s} PSD(\omega^s) \tag{15}$$

Figure 3 shows the approximate noise spectra for the SMC006 nozzle[27] predicted with the proposed acoustic-analogy approach, highlighting the agreement between the computed and expected decay at the higher frequencies.[33]

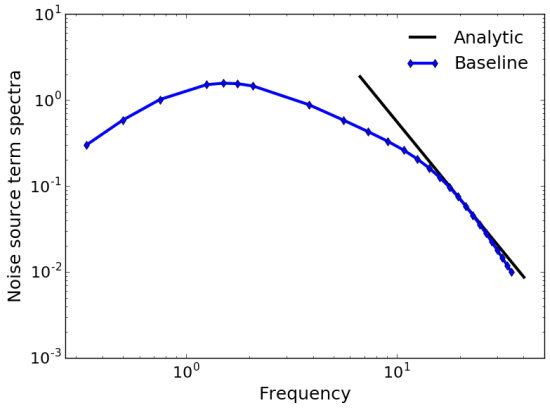

Figure 3. Approximate noise spectra for the baseline SMC006 nozzle geometry

Upon successful implementation of the proposed acoustic-analogy approach, the discrete tangent and adjoint linearizations of equations (11-15) have been implemented in order to enable the adjoint-based multidisciplinary shape optimization of the nozzle. Both tangent and adjoint linearizations are performed through exact hand differentiation of the acoustic source term and objective. Verification of the tangent linearization with respect to the complex-step differentiation[36] is presented in Table 1, showing machine precision agreement between these two approaches. The

Table 1. Verification of tangent sensitivity of equation (11) by complex step differentiation

Complex	1.0642623294695**77**E+05
Tangent	1.0642623294695**80**E+05

adjoint implementation has been verified by the duality relation[22] to the tangent approach as shown in Table 2.

Table 2. Verification of the adjoint sensitivity by duality relation with tangent linearization

Tangent	3.72684239789964E+09
Adjoint	3.72684239789963E+09

IV. Geometry Parametrization

To perform shape optimization of the nozzle geometry, the geometry shape parameters used are essentially of three kinds: chevron radial penetration (D_{rad}), chevron twist (D_ϕ) in nozzle azimuthal plane, and chevron length (D_l). Both axisymmetric and asymmetric twist types are incorporated. The radial penetration design parameter, $D_{rad_i} = \alpha_i$, is essentially the coefficient of a monomial function of i'th degree for a penetration in the radial direction ($\hat{e}_r$). The twist design variable, D_ϕ, is defined by the angle ($\Delta\phi$) by which the chevrons are twisted about the nozzle axis. The length design variable, D_l, corresponds to the relative change of the chevron base geometry (Δl) along the nozzle axis ($\hat{e}_a$). The combined deformation of a generic point ($\vec{x}$) due to all the design variables is given as:

$$\vec{x}_{def} - \vec{x}_{min} = \alpha_i \left[max\left((\vec{x} - \vec{x}_{min}) \cdot \hat{e}_a,\ 0.0\right)\right]^i \hat{e}_r \tag{16}$$

$$+ \left[R(\Delta\phi')\right](\vec{x} - \vec{x}_{min}) \tag{17}$$

$$+ \left[(\beta_l(\vec{x})\Delta l)\right]\hat{e}_a \tag{18}$$

where, $\left[R(\Delta\phi')\right]$ is the rigid rotation matrix for an angle of $\Delta\phi' = [\beta_\phi(\vec{x})][\gamma_\phi(\vec{x})]\Delta\phi$. The analytic function $\beta_\phi \in [0,1]$ ensures smooth twist along chevron length and the analytic function $\gamma_\phi \in [0,1]$ introduces asymmetric twist along

the nozzle azimuth. Similarly, the analytic function $\beta_l(\vec{x})$ ensures smooth nozzle length deformations. The nozzle deformations corresponding to each of the design variables are shown in Fig. 4.

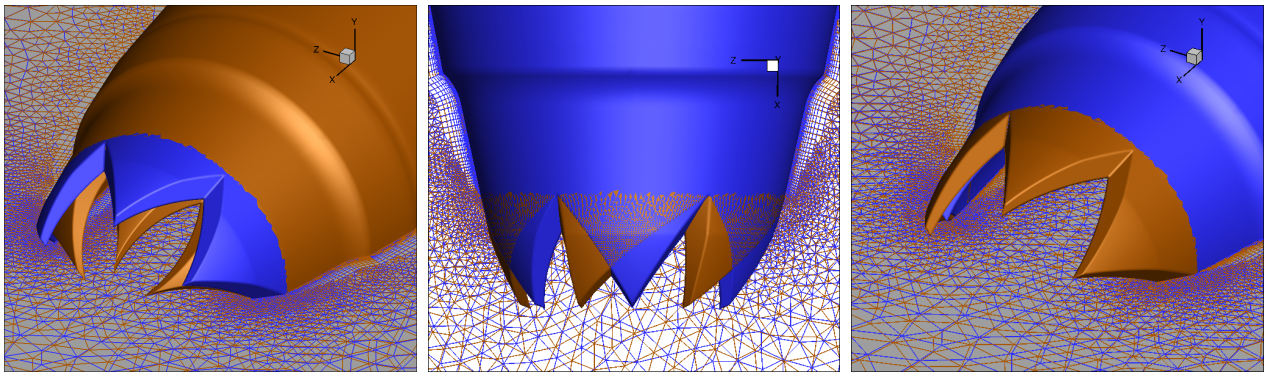

(a) Chevron penetration (b) Chevron twist (c) Nozzle length

Figure 4. Nozzle design variables; Blue: baseline, Orange: deformed

V. Optimization Results

The goal of the present work is to reduce the noise signature of the baseline SMC006 nozzle without compromising its aerodynamic performance. The discrete adjoint linearization of the acoustic-analogy approach presented in Sec. III is harnessed by the SNOPT gradient-based optimization method[37] to minimize the noise signature of the nozzle. The design variables used for the optimizations are the penetration and twist of the chevrons as well as the length of the nozzle, as discussed in Sec. IV. Three different design optimization studies are presented next. An aerodynamic optimization aims at maximizing the aerodynamic performance of the nozzle and the design optimization problem is

$$\min_{\mathbf{D}} \; L_{aero} \tag{19}$$

where $L_{aero} = C_d^2$. Although the aerodynamic performance of the nozzle is more accurately determined by the thrust produced, directly computing thrust for a chevron nozzle is complicated by the choice of an exit plane of integration. An alternative approach consists of performing an axial momentum control volume analysis, where the change in momentum is equated to the force on the nozzle. If the inlet momentum and pressure forces are known, and the drag force on the nozzle is computed by surface integration, the thrust force can be obtained by the momentum balance. In the current approach, using the drag coefficient as a surrogate for nozzle performance or thrust is equivalent to assuming no changes occur at the inlet plane of the nozzle. In future work, a more consistent thrust objective will be constructed based on the axial momentum control volume analysis approach.

The aerodynamic performance of the resulting nozzle represents the maximum performance achievable with the current design variables, but it will come at the expense of an increased jet noise signature. Conversely, an acoustic optimization aims at identifying the maximum noise reduction that can be realized in the current optimization framework at the expense of the aerodynamic performance. The nozzle acoustic design optimization problem can be stated as

$$\min_{\mathbf{D}} \; L_{acou} \tag{20}$$

where L_{acou} is the acoustic objective function described in equation (15). Finally, an aeroacoustic optimization aims at reducing the noise of the nozzle while limiting the degradation of its aerodynamic performance. The aerodynamic constraint is enforced using a penalty function approach and the optimization problem is

$$\min_{\mathbf{D}} \; L_{tot} \tag{21}$$

where $L_{tot} = L_{acou} + \omega_{aero} L_{aero}$. The acoustic objective function L_{acou} is described in equation (15) while the aerodynamic constraint is

$$L_{aero} = (Cd - Cd_{baseline})^2 \tag{22}$$

where $Cd_{baseline}$ is the drag coefficient of the baseline SMC006 nozzle and $\omega_{aero} = 1.0 \times 10^{-6}$ is an optimization weight used to enforce the aerodynamic constraint. For each optimization, one design cycle corresponds to one flow solution and one adjoint solution and takes approximately 30 minutes of wall-clock time on 128 cores.

Convergence of the aerodynamic optimization, equation (19), is shown in Fig. 5. Optimality, a measure of the gradients of the optimization objective function as computed by the optimizer SNOPT,[37] is reduced by more than three orders of magnitude in 20 design cycles, while the drag coefficient is reduced by 2.7% after just 5 design cycles. However, this aerodynamic improvement comes at a significant acoustic penalty, as shown in Fig. 5(c), suggesting that aerodynamic and noise objectives have opposing design requirements. Figure 6 summarizes the optimized nozzle shape. The chevrons are bent radially outward from the nozzle axis, while chevron twist and length play a minor role in the optimization.

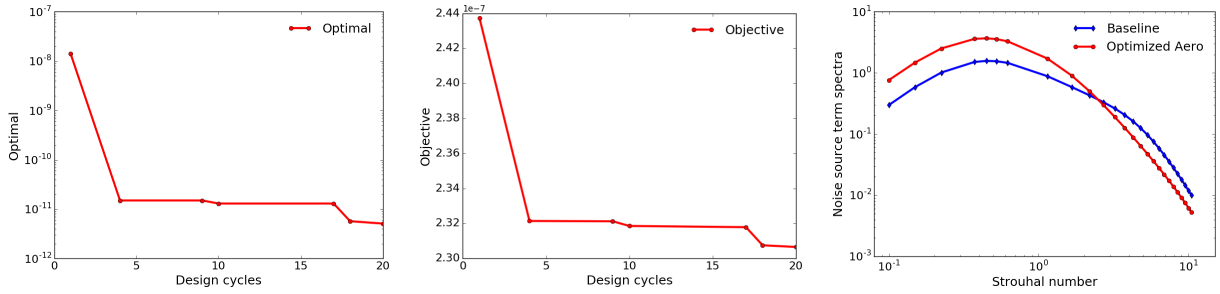

(a) Optimality (b) Objective (c) Noise

Figure 5. Unconstrained aerodynamic optimization convergence and noise penalty

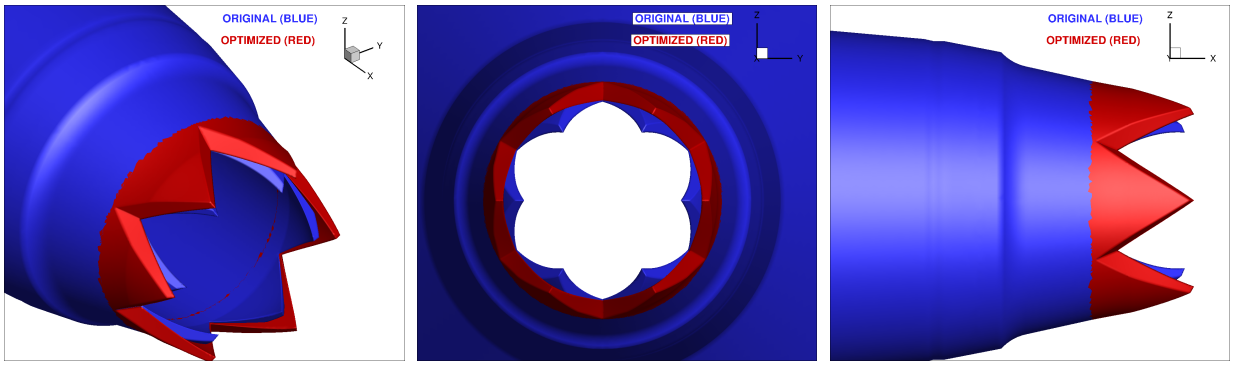

(a) Deformed geometry (b) Deformed geometry - top view (c) Deformed geometry - side view

Figure 6. Aerodynamic optimization deformations; Blue: original, Red: optimized

The results for the acoustic optimization described by equation (20), are presented next. Convergence of the optimization is shown in Fig. 7. After 7 design cycles, optimality is reduced 3 orders of magnitude, with the acoustic objective function that experiences its most significant reduction in only two design cycles. The noise source term spectra for the baseline and optimized nozzles are shown in Fig. 8, highlighting the significant noise reduction at the lower frequencies with only a marginal noise increase at the higher frequencies. Figure 9 shows that the noise reduction is achieved with increased chevron penetration in agreement with previous experimental and computational design studies,[27,38] while chevron twist and nozzle length again play a minimal role in the optimization. These results represent the maximum noise reduction achievable with the current design variables for the SMC006 nozzle and demonstrate the feasibility of the aeroacoustic adjoint approach and its ability to capture the correct acoustic design sensitivities. However, the achieved noise reduction compromises the aerodynamic performance of the nozzle resulting in a 3.3% increase in drag coefficient, confirming that acoustic and aerodynamic objectives have conflicting design requirements.

Finally, results for the aeroacoustic design optimization, equation (21), are presented next. Convergence of the optimization problem is shown in Fig. 10 and is achieved after 25 design cycles, with the objective function that settles after only 2 design cycles. Figure 10(c) compares the noise spectral densities for the baseline nozzle to the spectra from the aerodynamic optimization, the acoustic optimization, and the aeroacoustic optimization. The introduction

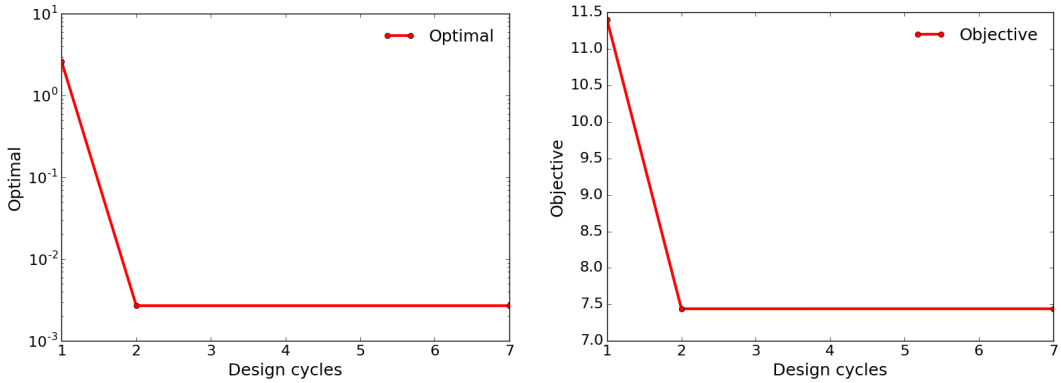

(a) Optimality (b) Objective function

Figure 7. Acoustic optimization convergence: a) Optimality as computed by SNOPT and b) optimization objective as function of design cycles

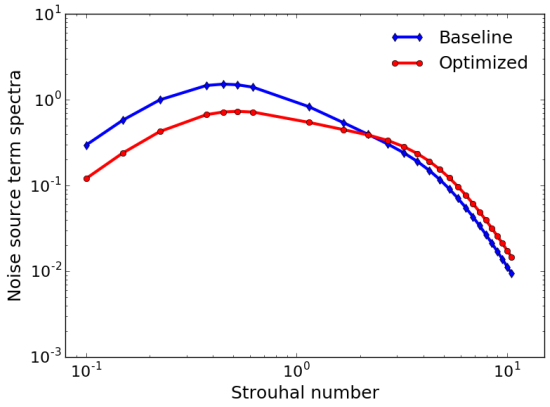

Figure 8. Spectra of the baseline and optimized nozzle

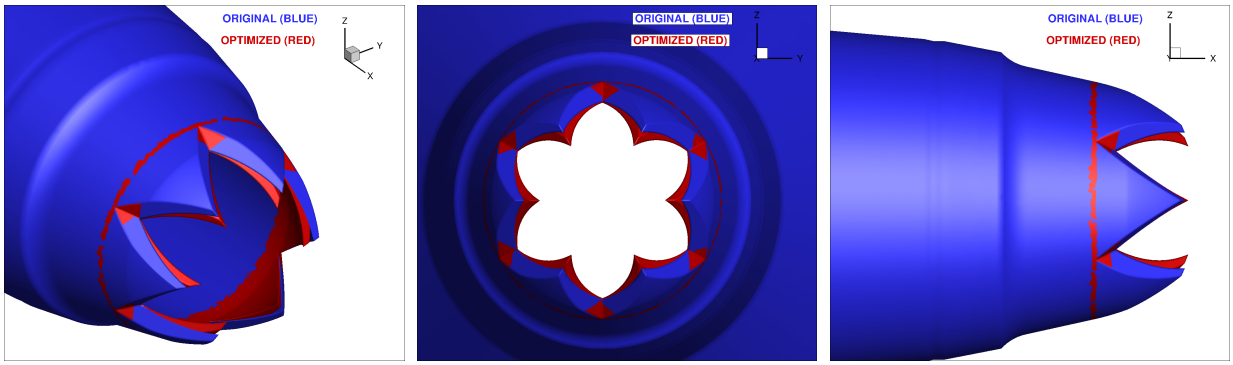

(a) Deformed geometry (b) Deformed geometry - top view (c) Deformed geometry - side view

Figure 9. Nozzle shapes for the baseline and acoustically optimized nozzles.

of the aerodynamic constraint results in a less effective noise minimization compared to the acoustic optimization. However, the drag coefficient of the nozzle increases by only 1.9% with respect to the baseline nozzle, as summarized in Table 3. The shape of the optimized nozzle is presented in Fig. 11 and is characterized by enhanced penetration of the nozzle with no significant chevron twist or length variation.

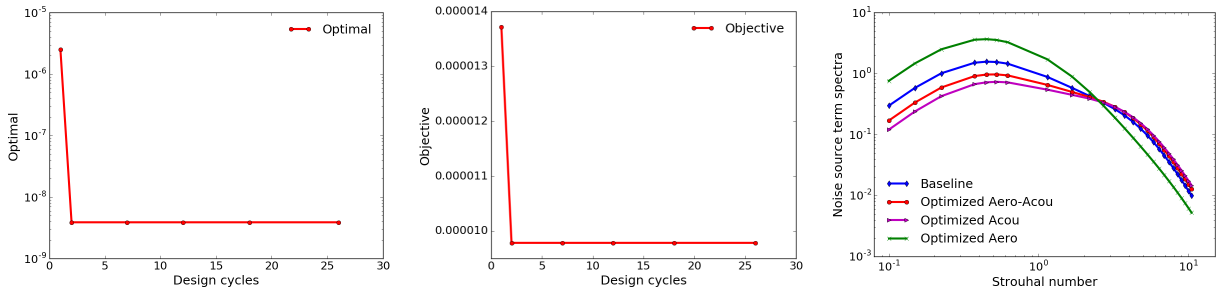

(a) Optimality (b) Function/Adjoint evaluations (c) Noise

Figure 10. Aero-acoustic optimization convergence and noise signatures.

Table 3. Drag comparison from optimizations

Cases	ΔC_d
Baseline (*BL*)	–
Aerodynamic Opt	-2.7 %
Acoustic Opt	+3.3 %
Aero-acoustic Opt	+1.9 %

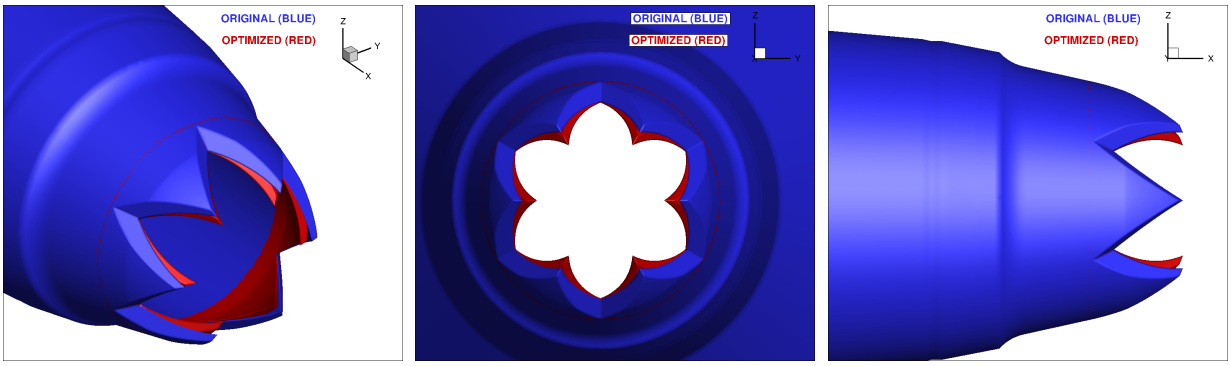

(a) Deformed geometry (b) Deformed geometry - top view (c) Deformed geometry - side view

Figure 11. Baseline and aeroacoustically optimized nozzles

These optimization results show the conflicting design requirements for nozzle noise reduction and aerodynamic performance and highlight the need for a multidisciplinary design optimization methodology capable of rapidly identifying the optimal shape of the nozzle.

A. Jet Noise Predictions with JeNo

The simplified acoustic analogy proposed in this work has been shown to be capable of capturing the noise design trends identified in previous experimental campaigns.[27] However, as part of an ongoing effort to develop an adjoint-based sensitivity analysis capability for NASA's JeNo software,[33,35] the noise reductions computed with the proposed acoustic approach have been verified by computing the far-field noise levels of the optimized nozzles using the JeNo code. Based on Lilley's acoustic analogy, the JeNo code assembles the acoustic source term described in equation (11) using a steady RANS solution on a structured mesh that extends downstream of the nozzle exit. Propagation of the nozzles' noise signatures to the far-field observer is accomplished using a Green's function approach.
The unstructured RANS solutions computed with the NSU3D flow solver are interpolated onto JeNo's structured mesh

using the TIOGA overset domain connectivity algorithm.[39,40] Upon interpolation, the JeNo code propagates the noise spectra to a 90-degree observer at a distance of 40 equivalent jet diameters from the nozzle.[27] Figure 12 compares the 1/3-octave spectrum computed with JeNo with the noise spectrum measured in the acoustic experiment for the baseline SMC006 nozzle.[27] There is reasonable agreement between computed and measured spectra, establishing confidence

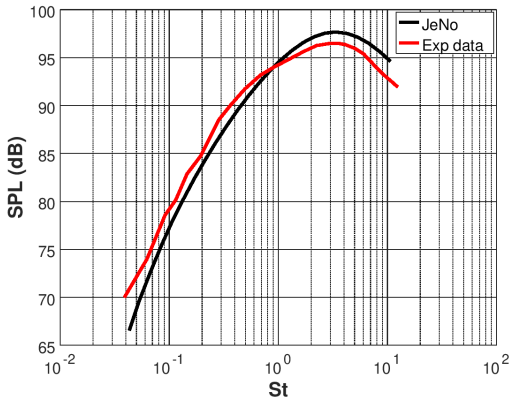

Figure 12. Comparison between measured and computed 1/3-octave unattenuated spectra for the baseline SMC006 chevron nozzle.

in both the NSU3D CFD solution and the 'NSU3D-TIOGA-JeNo' noise prediction strategy. Figure 13 compares the narrow-band spectra for the baseline SMC006 and the three optimized nozzles. The JeNo noise spectra confirm the results of the optimizations and demonstrate the ability of the proposed acoustic-analogy approach to capture the correct jet noise design trends for 90-degree observers.

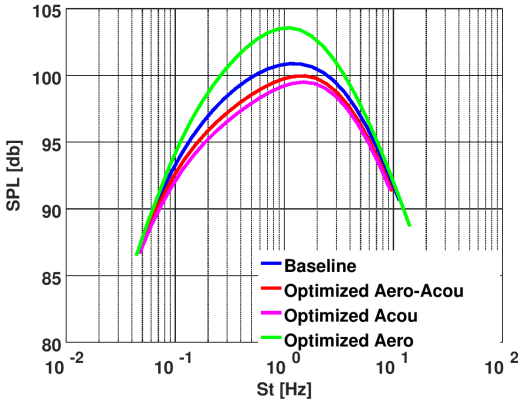

Figure 13. Narrow-band spectra computed with JeNo for the baseline and the three optimized nozzles.

VI. Conclusions and Future Work

A simplified acoustic analogy approach for supersonic jet noise has been implemented in this work. The proposed acoustic analogy has been enhanced with a discrete adjoint linearization to enable efficient multidisciplinary nozzle design optimization. The new adjoint formulation has been applied to the noise minimization of the SMC006 nozzle with minimal aerodynamic performance penalty. The optimization results demonstrate the feasibility of using an acoustic-analogy formulation to optimize nozzle jet noise using an adjoint-enabled gradient-based method. Future work will focus on replacing the simplified acoustic-analogy approach proposed in this work with the formulation available in the JeNo acoustic software, and on the implementation of the corresponding discrete adjoint operator.

VII. Acknowledgements

The authors would like to acknowledge support of NASA through NASA SBIR 2018 Phase-I funding, Contract: 80NSSC18P1888, Proposal: 18-1- A1.04-5483.

References

[1]Maglieri, D. J., Bobbit, P. J., Plotkin, K. J., Sheperd, K. P., Coen, P. G., and Richwine, D. M., "Sonic Boom - Six Decades of Research," Tech. Rep. SP-2014-622, NASA, 2014.

[2]Park, M. and Morgenstern, J. M., "Summary and Statistical Analysis of the First AIAA Sonic Boom Prediction Workshop," *Journal of Aircraft*, Vol. 53-2, 2016.

[3]Park, M. and Nemec, M., "Nearfield Summary and Statistical Analysis of the Second AIAA Sonic Boom Prediction Workshop," *Journal of Aircraft*, Vol. 56-3, 2019.

[4]Rallabahndi, S. K. and Loubeau, A., "Summary of Propagation Cases of the Second AIAA Sonic Boom Prediction Workshop," *Journal of Aircraft*, Vol. 56-3, 2019.

[5]Rallabahndi, S. K., Nielsen, E., and Diskin, B., "Sonic-Boom Mitigation Through Aircraft Design and Adjoint Methodology," *Journal of Aircraft*, Vol. 51-2, 2014.

[6]Minelli, A., el Din, I. S., and Carrier, G., "Inverse Design Approach for Low-Boom Supersonic Configurations," *AIAA Journal*, Vol. 52-10, 2014.

[7]Housman, J. A., Stich, G.-D., Kiris, C. C., and Bridges, J., "Jet Noise Prediction using Hybrid RANS/LES with Structured Overset Grids," *23rd AIAA/CEAS Aeroacoustics Conference*, June 5–9 2017, AIAA Paper 2017–3213.

[8]Stich, G.-D., Housman, J. A., Kocheemoolayil, J. G., Kiris, C. C., Bridges, J., and Brown, C. A., "Hybrid RANS/LES Simulation of Jet Surface Interaction Noise," *25th AIAA/CEAS Aeroacoustics Conference*, May 20–23 2019, AIAA Paper 2019–2475.

[9]Khavaran, A., Kenzakowski, D. C., and Mielke-Fagan, A. F., "Hot Jets and Sources of Jet Noise," *International Journal of Aeroacoustics*, Vol. 9, No. 4-5, 2010, pp. 491–532.

[10]Bridges, J., Khavaran, A., and Hunter, C. A., "Assessment of Current Jet Noise Prediction Capabilities," NASA/TM 2008-215275.

[11]Jameson, A., "Aerodynamic Shape Optimization using the Adjoint Method," *VKI Lecture Series on Aerodynamic Drag Prediction and Reduction, von Karman Institute of Fluid Dynamics, Rhode St Genese, Belgium*, 2003.

[12]Martins, J. R. R. A. and Lambe, A. B., "Multidisciplinary Design Optimization: A Survey of Architectures," *AIAA Journal*, Vol. 51, 2013, pp. 2049–2075.

[13]Mishra, A., Mani, K., Mavriplis, D. J., and Sitaraman, J., "Time-dependent Adjoint-based Aerodynamic Shape Optimization Applied to Helicopter Rotors," *Journal of Computational Physics*, Vol. 292, No. 1, 2015, pp. 253–271, doi:10.1016/j.jcp.2015.03.010.

[14]Mishra, A., Mavriplis, D., and Sitaraman, J., "Time-dependent aeroelastic adjoint-based aerodynamic shape optimization of helicopter rotors in forward flight," *AIAA Journal*, 2016, pp. 3813–3827.

[15]Rumpfkeil, M. and Zingg, D., "The Optimal Control of Unsteady Flows With a Discrete Adjoint Method," *Journal of Optimization and Engineering*, Vol. 11, No. 1, 2010, pp. 5–22.

[16]Fabiano, E., Mavriplis, D. J., and Sitaraman, J., "Adjoint - based Aeroacoustic Design Optimization for Blade Vortex Interaction Noise," *53rd AIAA Aerospace Sciences Meeting*, January 4–8 2015, AIAA Paper 2015–1801.

[17]Fabiano, E., Mishra, A., Mavriplis, D. J., and Mani, K., "Time-dependent aero-acoustic adjoint-based shape optimization of helicopter rotors in forward flight," *57th AIAA/ASCE/AHS/ASC Structures, Structural Dynamics, and Materials Conference*, 2016, p. 1910.

[18]Fabiano, E. and Mavriplis, D., "Adjoint-Based Aeroacoustic Design-Optimization of Flexible Rotors in Forward Flight," *Journal of the American Helicopter Society*, Vol. 62, No. 4, 2017, pp. 1–17.

[19]Bridges, J., "Rapid Prediction of Installed Jet Noise from RANS," *25th AIAA/CEAS Aeroacoustic Conference*, May 20–23 2019.

[20]Khavaran, A., Bridges, J., and Freund, B. J., "A Parametric Study of Fine-Scale Turbulence Mixing Noise," NASA/TM 2002-211696.

[21]Khavaran, A., "Role of Anisotropy on Turbulent Mixing Noise," *AIAA Journal*, Vol. 37-7, 1999.

[22]Mavriplis, D. J., "Discrete Adjoint-Based Approach for Optimization Problems on Three-Dimensional Unstructured Meshes," *AIAA Journal*, Vol. 45-4, April 2007, pp. 741–750.

[23]Mavriplis, D. J., "Solution of the Unsteady Discrete Adjoint for Three-Dimensional Problems on Dynamically Deforming Unstructured Meshes," *Proceedings of the 46th Aerospace Sciences Meeting and Exhibit, Reno NV*, 2008, AIAA Paper 2008–0727.

[24]Mani, K. and Mavriplis, D. J., "Geometry Optimization in Three-Dimensional Unsteady Flow Problems using the Discrete Adjoint," *51st AIAA Aerospace Sciences Meeting, Grapevine, TX*, January 2013, AIAA Paper 2013-0662.

[25]Mavriplis, D. J., "Unstructured-Mesh Discretizations and Solvers for Computational Aerodynamics," *AIAA Journal*, Vol. 46-6, June 2008, pp. 1281–1298.

[26]Mavriplis, D. J., "Multigrid Strategies for Viscous Flow Solvers on Anisotropic Unstructured Meshes," *Journal of Computational Physics*, Vol. 145, No. 1, Sept. 1998, pp. 141–165.

[27]Bridges, J. and Brown, C. A., "Parametric Testing of Chevrons on Single Flow Hot Jets," *AIAA Paper 2004-2824, 10th AIAA/CEAS Aeroacoustic Conference, Manchester, GB*, May 2004, AIAA Paper 2004-2824.

[28]Tanna, H. K., Dean, P. D., and J., F. M., "The Influence of Temperature on Shock-Free Supersonic Jet Noise," *Journal of Sound and Vibration*, Vol. 39, No. 4, 1975, pp. 429–460.

[29]Dippold, V. F., "Generating a Grid for Unstructured RANS Simulations of Jet Flows," *2018 Fluid Dynamics Conference*, 2018, p. 3223.

[30]Yang, Z. and Mavriplis, D. J., "A Mesh Deformation Strategy Optimized by the Adjoint Method on Unstructured Meshes," *AIAA Journal*, Vol. 45, No. 12, 2007, pp. 2885–2896.

[31]Mavriplis, D. J., Yang, Z., and Long, M., "Results using NSU3D for the first Aeroelastic Prediction Workshop," *Proceedings of the 51st Aerospace Sciences Meeting and Exhibit, Grapevine TX*, 2013, AIAA Paper 2013–0786.

[32]Leib, S. J. and Goldstein, M. E., "Hybrid Source Modeling for Predicting High-Speed Jet Noise," *AIAA Journal*, Vol. 49, 2011, pp. 1324–1335.

[33]Khavaran, A., Bridges, J., and Georgiadis, N., "Prediction of Turbulence-Generated Noise in Unheated Jets. Part 1: JeNo Technical Manual," NASA/TM 2005-213827.

[34]Khavaran, A. and Bridges, J., "An Empirical Temperature Variance Source Model in Heated Jets," NASA/TM 2012-217743.

[35]Khavaran, A., Wolter, J. D., and Koch, D. L., "Prediction of Turbulence-Generated Noise in Unheated Jets. Part 2: JeNo User's Manual (Version 1.0)," NASA/TM—2009-213827/PART2.

[36]Martins, J. R. R. A. S. P. and Alonso, J. J., "The Complex-Step Derivative Approximation," *ACM Transactions on Mathematical Software*, Vol. 29-3, 2003, pp. 245–262.

[37]Gill, P. E., Murray, W., and Saunders, M. A., "SNOPT: An SQP Algorithm for Large-Scale Constrained Optimization," *SIAM review*, Vol. 47-1, 2005, pp. 99–131.

[38]Engblom, W. A., Khavaran, A., and Bridges, J., "Numerical Prediction of Chevron Nozzle Noise Reduction using WIND-MGBK Methodology," *AIAA Paper 2004-2979, 10th AIAA/CEAS Aeroacoustic Conference, Manchester, GB*, May 2004, AIAA Paper 2004-2979.

[39]Roget, B. and Sitaraman, J., "Robust and efficient overset grid assembly for partitioned unstructured meshes," *Journal of Computational Physics*, Vol. 260, 2014, pp. 1–24.

[40]Brazell, M. J., Sitaraman, J., and Mavriplis, D. J., "An overset mesh approach for 3D mixed element high-order discretizations," *Journal of Computational Physics*, Vol. 322, 2016, pp. 33–51.